HHS Public Access

Author manuscript

J Proteome Res. Author manuscript; available in PMC 2024 October 05.

Published in final edited form as:

J Proteome Res. 2024 January 05; 23(1): 356–367. doi:10.1021/acs.jproteome.3c00600.

Expression of SARS-CoV-2 Nonstructural Proteins 3 and 4 Can Tune the Unfolded Protein Response in Cell Culture

Jonathan P. Davies[⊥],
Department of Biological Sciences, Vanderbilt University, Nashville, Tennessee 37240, United States

Athira Sivadas[⊥],
Department of Biological Sciences, Vanderbilt University, Nashville, Tennessee 37240, United States

Katherine R. Keller,
Department of Pharmacology, SUNY Upstate Medical University, Syracuse, New York 12310, United States

Brynn K. Roman,
Department of Biological Sciences, Vanderbilt University, Nashville, Tennessee 37240, United States

Richard J.H. Wojcikiewicz,

Corresponding Author: Lars Plate – Department of Biological Sciences and Department of Chemistry, Vanderbilt University, Nashville, Tennessee 37240, United States; Department of Pathology, Microbiology and Immunology, Vanderbilt University Medical Center, Nashville, Tennessee 37240, United States; lars.plate@vanderbilt.edu.

Author Contributions

J.P.D., A.S., and L.P.: conceptualization; J.P.D., A.S., and L.P.: formal analysis; J.P.D., A.S., and L.P.: methodology; J.P.D., A.S., K.R.K., and B.K.R.: investigation; R.J.H.W. and L.P.: supervision; J.P.D., A.S., and L.P.: writing – original draft; J.P.D., A.S., L.P., B.K.R., K.R.K., and R.J.H.W.: writing – review and editing.

[⊥]J.P.D. and A.S. contributed equally.

Supporting Information

The Supporting Information is available free of charge at https://pubs.acs.org/doi/10.1021/acs.jproteome.3c00600.

Supplemental Figure S1: western blot analysis of HEK293T cells transfected with specified viral proteins or Tdtomato as basal control; Supplemental Figure S2: western blot analysis of HEK293T cells transfected with specified viral proteins and blotted for CHOP and BiP; Supplemental Figure S3: effect of PERK inhibition on ATF4 upregulation mediated by nsp4; Supplemental Figure S4: TMT abundances of proteins identified by mass spectrometry in this study; Supplemental Figure S5: waterfall plot of proteome in HEK293T cells expressing SARS-CoV-2 nsp4-ST vs GFP control; Supplemental Figure S6: normalized TMT abundance levels of individual UPR pathway protein markers in HEK293T cells expressing various viral proteins; Supplemental Figure S7: ATF6 marker enrichment for with treatment of Tm, 147, or nsp4-ST expression; Supplemental Figure S8: effect of various multipass transmembrane proteins on the UPR as compared to nsp4; Supplemental Figure S9: global proteome analysis of A549 cells expressing SARS-CoV-2 nsp4-FT vs GFP control; Supplemental Figure S10: normalized TMT abundance levels of individual UPR pathway protein markers in A549 cells expressing nsp4-FT or treated with Tm; Supplemental Figure S11: western blot analysis of HEK293T cells transfected with specified viral proteins and blotted for ATF6 protein markers; Supplemental Figure S12: upregulation of IRE/XBP1s proteomics protein markers; Supplemental Figure S13: viral protein abundance levels when expressed in HEK293T cells (PDF)

Supplemental Table S1 of UPR pathway protein sets used for proteomics analysis (XLSX)

Supplemental Table S2 of proteins identified by LC/MS-MS in HEK293T cells (XLSX)

Supplemental Table S3 of peptides identified by LC/MS-MS in HEK293T cells (XLSX)

Supplemental Table S4 of proteins identified by LC/MS-MS for Transmembrane Protein panel (XLSX)

Supplemental Table S5 of peptides identified by LC/MS-MS for Transmembrane Protein panel (XLSX)

Supplemental Table S6 of proteins identified by LC/MS-MS in A549 cells (XLSX)

Supplemental Table S7 of peptides identified by LC/MS-MS in A549 cells (XLSX)

Complete contact information is available at: https://pubs.acs.org/10.1021/acs.jproteome.3c00600

The authors declare no competing financial interest.

Department of Pharmacology, SUNY Upstate Medical University, Syracuse, New York 12310, United States

Lars Plate
Department of Biological Sciences and Department of Chemistry, Vanderbilt University, Nashville, Tennessee 37240, United States; Department of Pathology, Microbiology and Immunology, Vanderbilt University Medical Center, Nashville, Tennessee 37240, United States

Abstract

Coronaviruses (CoV), including SARS-CoV-2, modulate host proteostasis through the activation of stress-responsive signaling pathways such as the Unfolded Protein Response (UPR), which remedies misfolded protein accumulation by attenuating translation and increasing protein folding capacity. While CoV nonstructural proteins (nsps) are essential for infection, little is known about the role of nsps in modulating the UPR. We characterized the impact of overexpression of SARS-CoV-2 nsp4, a key driver of replication, on the UPR in cell culture using quantitative proteomics to sensitively detect pathway-wide upregulation of effector proteins. We find that nsp4 preferentially activates the ATF6 and PERK branches of the UPR. Previously, we found that an N-terminal truncation of nsp3 (nsp3.1) can suppress pharmacological ATF6 activation. To determine how nsp3.1 and nsp4 tune the UPR, their coexpression demonstrated that nsp3.1 suppresses nsp4-mediated PERK, but not ATF6 activation. Reanalysis of SARS-CoV-2 infection proteomics data revealed time-dependent activation of PERK targets early in infection, which subsequently fades. This temporal regulation suggests a role for nsp3 and nsp4 in tuning the PERK pathway to attenuate host translation beneficial for viral replication while avoiding later apoptotic signaling caused by chronic activation. This work furthers our understanding of CoV-host proteostasis interactions and highlights the power of proteomic methods for systems-level analysis of the UPR.

Graphical Absrtract

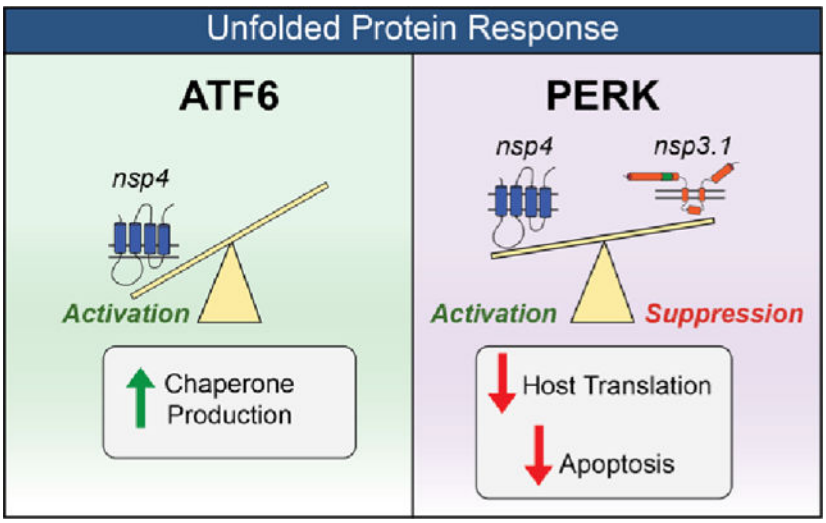

Keywords

coronavirus; proteomics; stress response; nonstructural protein; ATF6; PERK

INTRODUCTION

The coronavirus SARS-CoV-2 has caused the COVID-19 pandemic, resulting in more than 6.8 million deaths to date.[1] Coronaviruses (CoV) require host cell translation machinery and endoplasmic reticulum (ER) derived membranes for replication. CoV infection is known to induce ER stress and activate the Unfolded Protein Response (UPR).[2–4] The UPR alleviates stress from accumulation of misfolded proteins in the ER lumen by temporarily suppressing global protein translation, increasing the production of ER chaperones, expanding ER membrane synthesis, and, if stress persists, triggering apoptosis. The UPR is composed of three branches that signal downstream of their respective ER-membrane localized stress sensors: (1) protein kinase R-like ER kinase (PERK), (2) inositol requiring enzyme 1α (IRE1α), and (3) activating transcription factor 6 (ATF6) pathways.[5,6]

Activation of PERK leads to the phosphorylation of eukaryotic initiation factor 2α (eIF2α) and attenuation of global protein translation to prevent further accumulation of misfolded proteins in the ER. A select group of proteins are translated under these conditions, including activating transcription factor 4 (ATF4), which upregulates expression of various genes involved in protein folding, antioxidant response, and the pro-apoptotic transcription factor C/EBP Homologous Protein (CHOP).[7,8] IRE1α has endoribonuclease activity, which, upon ER stress, cleaves X-box-binding protein 1 (*XBP1*) transcripts, leading to splicing and translation of the XBP1s transcription factor and increased gene expression of ER protein chaperones, translocation and secretion factors, and components of ER-associated degradation (ERAD) as well as ER biogenesis.[9] Lastly, ATF6 is translocated to the Golgi upon ER stress, where it is cleaved by site-1 and site-2-proteases. The N-terminal fragment (ATF6p50) is a transcription factor, which initiates upregulation of various protein folding, secretion, and degradation factors as well as expansion of the ER.[5,6,10,11]

Coronavirus replication requires extensive production, folding, and modification of viral proteins,[12] as well as alteration of ER-derived membranes to form double-membrane vesicles (DMVs) for replication sites. These processes can trigger ER stress and activate the UPR.[13] Indeed, a previous study found that all three branches of the UPR are activated during SARS-CoV-2 infection and that expression of SARS-CoV-2 Spike or orf8 protein is sufficient to activate the UPR[3]. SARS-CoV proteins orf3a and orf8ab were also found to activate the PERK and ATF6 pathways, respectively.[14,15] A related betacoronavirus, mouse hepatitis virus (MHV), triggers the activation of XBP1 and PERK pathways while also hindering production of certain UPR-responsive genes such as CHOP[4]. This previous work shows that coronaviruses can modulate stress responses at multiple phases and emphasizes the need for downstream proteome measurements to elucidate the consequences in the host cell.

Surprisingly, relatively little is known about the impact of CoV nonstructural proteins (nsps) on the UPR. Nsps are the first viral proteins translated during infection that rewire the host cell and replicate the viral genome. In particular, three transmembrane nsps (nsp3, nsp4, and nsp6) are responsible for DMV formation from ER-derived membranes.[16] Nsp3 contains a papain-like protease domain ($PL2^{pro}$), which cleaves the orf1a/b polypeptide and also

possesses deubiquination/de-ISGylation activity.[17,18] Nsp4 is a glycoprotein containing four transmembrane domains and plays a key role in membrane reorganization.[19,20]

We have previously characterized the interactomes of nsp3 and nsp4 CoV homologues and found that both proteins have evolutionary conserved interactions with several ER proteostasis factors.[21,22] We identified an interaction between an N-terminal fragment of SARS-CoV-2 nsp3 (nsp3.1) and ATF6 and showed that nsp3.1 can suppress pharmacologic activation of the ATF6 pathway.[22] Given the known role of nsp4 in host membrane alteration, we sought to elucidate if nsp4 activates or suppresses the UPR and whether nsp4 may act in concert with nsp3 to tune UPR activation. In particular, we leveraged a quantitative proteomics approach to characterize the upregulation of genes known to be transcriptionally activated by the UPR.[6,23,24] Importantly, this approach enables sensitive measurement of pathway-wide changes in effector proteins and accounts for viral protein-mediated regulation that may occur downstream of transcriptional activation. A more precise understanding of the role of CoV nsps in modulating the UPR will further our understanding of how coronavirus replication manipulates host proteostasis pathways during infection.

EXPERIMENTAL SECTION

DNA Constructs

SARS-CoV-2 nsp4-FT, nsp3-FT, FT-nsp2, and orf8-FT (Wuhan-Hu-1 MN908947) were codon-optimized and cloned into a pcDNA-(+)-C-DYK vector (Genscript) or a pcDNA-(+)-N-DYK vector for nsp2 (Genscript). An N-terminal truncation nsp3.1-FT (residues 1–749) was generated as previously described.[21] Nsp4-ST and orf8-ST constructs were generated through the NEB HiFi Assembly system. In brief, the FLAG-tag from nsp4-FT was removed through amplification with primers 3 and 4 respectively. A 2xStrepTag was amplified from a SARS-CoV-2 nsp2-ST in a pLVX-EF1alpha plasmid construct (kind gift from Dr. Nevan Krogan, University of California, San Francisco) using primers 1 and 2. The linear nsp4 product was then combined with the 2xStrepTag fragment via HiFi assembly (1:2 vector to insert ratio). The orf8-ST construct was made by amplifying out the orf8 gene from the pcDNA-(+)-C-DYK vector using primers 5 and 6. A pLVX-EF1alpha-SARS-CoV-2-nsp2-2xStrepTag plasmid was linearized using primers 7 and 8, retaining the vector backbone and 2xStrepTag while removing the nsp2 gene. These were then combined via HiFi assembly (1:2 vector to insert ratio). A plasmid expressing human WT CFTR in the pcDNA5 vector was gifted from Dr. Eric Sorscher and Jeong Hong (Emory University).[25] The expression plasmid for human ERG (KCNH2) with an HA-tag in the first extracellular loop (residues 444–460) in a pAG293-pIRES2-GFP backbone was provided by Dr. Brett Kronke (Vanderbilt University Medical Center).[26] The expression plasmid for human PMP22 with a Myc-tag in the second extracellular loop (residues 126–135) in a pIRES2-EGFP vector was provided by Dr. Charles Sanders (Vanderbilt University).[27] Plasmids were verified by sequencing (Genewiz) (Table 1).

Cell Culture and Transfection

HEK293T cells were generously provided by J. Genereux (University of California, Riverside). A549 lung epithelial cells were obtained from the ATCC (CCL-185). Cell

lines were tested regularly for mycoplasma. HEK293T and A549 cells were maintained at 37 °C and 5% CO_2 in high glucose Dulbecco's modified Eagle growth medium with 10% fetal bovine serum, 1% glutamine, and 1% penicillin/streptomycin (DMEM-10). Cells were seeded into 6-well plates at a concentration of 4×10^5 cells/well. HEK293T cells were transfected dropwise, 24 h after seeding, using a calcium phosphate cocktail (1.5 μg total DNA, 0.25 M $CaCl_2$, 1× HBS (137 mM NaCl, 5 mM KCl, 0.7 mM Na_2HPO_4 7.5 mM-glucose, 21 mM HEPES)). For PMP22-Myc expression, a lower DNA amount of 0.3 μg was used, as previously described.[27] The media were changed 18 h later with fresh DMEM-10 media. A549 cells were seeded in antibiotic-free DMEM-10 and 24 h later were transfected with a FuGENE 4K transfection reagent (FuGENE no. E5911) (1.5 μg DNA with 4.5 μL FuGENE 4K) in plain Optimem media. Samples were treated with DMSO or tunicamycin (Tm, 1 μg/mL) for 16 h (protein analysis) or 6 h (RNA analysis) prior to harvest in the described experiments. GFP controls were used to assess transfection efficiency, which averaged 70–80% in HEK293T cells and 40–50% in A549 cells. Transfected cells were harvested by cell scraping in cold 1 mM EDTA in PBS over ice 40 h post-transfection to enable robust expression of viral proteins. To measure CHOP levels, HEK293T cells were transfected 24 h after seeding, using 1 μg of cDNAs and 6 μL of 1 mg/mL PEI (premixed in 50 μL of serum-free culture medium). Samples were treated with tunicamycin (Tm, 5 μg/mL) for 4 or 20 h prior to harvest.

RT-qPCR

HEK293T cells were transfected and harvested as described above. Cellular RNA was extracted using the Zymo QuickRNA miniprep kit (#R1055) and 500 ng of total cellular RNA was reverse transcribed into cDNA using random hexamer primers (IDT #51–01–18–25), oligo-dT 15mer primers (IDT # 51–01–15–05), and Promega M-MLV reverse transcriptase (#M1701). qPCR analysis was carried out using BioRad iTaq Universal SYBR Green Supermix (no. 1725120), added to respective primers (primers 9–14) for target genes, and reactions were run in 96-well plates on a BioRad CFX qPCR instrument. Conditions used for amplification were 95 °C, 2 min, 45 repeats of 95 °C, 10 s, and 60 °C, 30 s. A melting curve was generated in 0.5 °C intervals from 65 to 95 °C. Cq values were calculated by the BioRad CFX Maestro software and transcripts were normalized to a housekeeping gene (*GAPDH*). All measurements were performed in technical duplicate; technical duplicates were averaged to form a single biological replicate.

PERK Inhibition Assay

HEK293T cells were seeded in 6-well plates at 4×10^5 cells/well and transfected with GFP or SARS-CoV-2 nsp4-FT as previously described. GFP samples treated with either tunicamycin (Tm, 1 μg/mL) or Tm and PERK inhibitor II GSK2656157 (PERKi, 1 μM) for 16 h and nsp4-FT samples treated with PERK inhibitor II GSK2656157 (PERKi, 1 μM) for 36h prior to harvest. Samples were harvested 40 h post-transfection by scraping and lysed in RIPA buffer as described in Western Blot Analysis.

Western Blot Analysis

HEK293T cells were lysed on ice in TNI buffer (50 mM Tris pH 7.5, 150 mM NaCl, 0.5% IGEPAL-CA-630) with Roche complete EDTA-free protease inhibitor (#4693132001)

for 15 min and then sonicated for 10 min in a water bath at room temperature. A549 cells were lysed on ice in RIPA buffer (50 mM Tris pH 7.5, 150 mM NaCl, 0.1% SDS, 1% Triton X-100, 0.5% deoxycholate) with Roche complete EDTA-free protease inhibitor (#4693132001) for 15 min. HEK293T cells for the transmembrane protein panel (CFTR, hERG-HA, PMP22-Myc, nsp4-ST) and PERK inhibition assay were also lysed in RIPA buffer. Lysates were spun down at 21,100*g* for 15 min at 4 °C. Samples were added to 6× Laemelli buffer (12% SDS, 125 mM Tris, pH 6.8, 20% glycerol, bromophenol blue, 100 mM DTT) and heated at 37 °C for thirty minutes. The samples were then run on an SDS-PAGE gel and transferred to a PVDF membrane for Western blotting. M2 anti-FLAG (Sigma Aldrich, F1804), anti-KDEL (Enzo ADI-SPA-827-F), anti-PDIA4 (ProteinTech 14712–1-AP), THE anti-Strep II tag FITC (Genescript, A01736–100), anti-CFTR (217) (University of North Carolina-Chapel Hill CFTR Antibody Distribution Program), anti-HA.11 (Biolegend, 901513), anti-Myc (9B11) (Cell Signaling Technology, 2276S), anti-GFP (ThermoFisher, A6455), anti-ATF4 (Cell Signaling Technology, 11815), or anti-GAPDH (GeneTex, GTX627408) antibodies were used to probe Western blots at a 1:1000 dilution in TBS blocking buffer (0.1% Tween, 5% BSA, 0.1% Sodium Azide).

To measure CHOP protein levels, HEK293T cells were lysed on ice in 1% CHAPS lysis buffer (50 mM Tris H-Cl, 150 mM NaCl, 1 mM EDTA, 1% CHAPS, 10 μM pepstatin, 0.2 mM phenylmethylsulfonyl fluoride, 0.2 μM soybean trypsin inhibitor, and 1 mM DTT; pH 8.0) for 30 min. Lysates were spun down at 16,000*g* for 10 min at 4 °C. Samples were added to 4× gel-loading buffer (50 mM Tris/HCl (pH 6.8), 100 mM DTT, 2% SDS, 0.1% bromophenol blue, 10% glycerol, 100 mM DTT) and heated at 37 °C for thirty minutes. The samples were then run on a 13% SDS-PAGE gel and transferred to a nitrocellulose membrane for western blotting. M2 anti-FLAG (Sigma Aldrich, F1804), anti-BiP #3177 (Cell Signaling Technology), anti-CHOP #7351, and anti-GAPDH #365062 (Santa Cruz Biotechnology Inc.) antibodies were used to probe western blots in a TBS blocking buffer (0.1% Tween, 4% BSA, 0.1% Sodium Azide). The GAPDH signal was used to normalize band intensities. Protein expression on western blots was quantified by using ImageLab.

Proteomics Experimental Design

HEK293T UPR analysis combined 2–3 biological replicates into 1 individual MS run (3× GFP, 3× nsp3.1-FT+GFP, 3× nsp4-ST+GFP, 3× nsp3.1-FT+nsp4-ST, 2× orf8-ST+GFP, 2× orf8-ST+nsp3.1-FT). A549 UPR analysis combined 4 biological replicates into 1 individual MS run (4× GFP, 4× GFP +Tm, 4× nsp4-FT). UPR analysis of transmembrane protein panel expression in HEK293T cells combined 3–4 biological replicates into 1 MS run (3× GFP, 4× WT-CFTR, 3× hERG-HA, 3× PMP22-Myc, 3× nsp4-ST).

Sample Preparation for Mass Spectrometry

Samples were harvested and lysed as described in Western Blot Analysis. Protein concentration was quantified using 1× BioRad Protein Assay Dye (#5000006), and 20 μg of protein from each sample was prepared for mass spectrometry. Proteins were precipitated via mass spectrometry grade methanol:chloroform:water (in a 3:1:3 ratio) and washed three times with methanol. Each wash was followed by a 2 min spin at 10,000*g* at room temperature. Protein pellets were air-dried for 30–45 min and resuspended in 5 μL of 1%

Rapigest SF (Waters #186002122). Resuspended proteins were diluted with 32.5 μL of water and 10 μL of 0.5 M HEPES (pH 8.0) and then reduced with 0.5 μL of freshly made 0.5 M TCEP for 30 min at room temperature. Samples were then alkylated with 1 μL of fresh 0.5 M iodoacetamide (freshly made) for 30 min at room temperature in the dark and digested with 0.5 μg of Pierce Trypsin/Lys-C (Thermo Fisher # A40007) overnight at 37 °C shaking. Peptides were diluted to 60 μL with LC/MS-grade water and labeled using TMTpro labels (Thermo Scientific # A44520) for 1 h at room temperature. Labeling was quenched with the addition of fresh ammonium bicarbonate (0.4% v/v final) for 1 h at room temperature. Samples were then pooled, acidified to pH < 2.0 using formic acid, concentrated to 1/6th the original volume via Speed-vac, and diluted back to the original volume with buffer A (95% water, 5% acetonitrile, 0.1% formic acid). Cleaved Rapigest products were removed by centrifugation at 17,000*g* for 30 min, and the supernatant was transferred to fresh tubes.

MudPIT LC-MS/MS Analysis

Alternating layers of 1.5 cm Aqua 5 μm C18 resin (Phenomenex # 04A-4299), 1.5 cm Luna 5 μm SCX resin (Phenomenex # 04A-4398), and 1.5 cm Aqua 5 μm C18 resin were packed to make triphasic MudPIT columns as described previously.[29] TMT-labeled samples (20 μg) were loaded onto the microcapillaries via a high-pressure chamber followed by a 30 min wash in buffer A (95% water, 5% acetonitrile, and 0.1% formic acid). The MudPIT columns were installed on the LC column switching valve followed by a 20 cm fused silica microcapillary column filled with Aqua C18, 3 μm resin (Phenomenex no. 04A-4311) ending in a laser-pulled tip. Columns were washed in the same way as the MudPIT capillaries prior to use. Liquid chromatography (Ultimate 3000 nanoLC system) was used to fractionate the peptides online and then analyze via an Exploris480 mass spectrometer (Thermo Fisher). MudPIT runs were carried out by 10 μL sequential injections of 0, 10, 20, 30, 40, 50, 60, 70, 80, 90, and 100% buffer C (500 mM ammonium acetate, 94.9% water, 5% acetonitrile, 0.1% formic acid) followed by a final injection of 90% C and 10% buffer B (99.9% acetonitrile, 0.1% formic acid v/v). Each injection was followed by a 130 min gradient using a flow rate of 500 nL/min (0–6 min: 2% buffer B, 8 min: 5% B, 100 min: 35% B, 105min: 65% B, 106–113 min: 85% B, 113–130 min: 2% B). ESI was performed directly from the tip of the microcapillary column using a spray voltage of 2.2 kV, an ion transfer tube temperature of 275 °C, and an RF Lens of 40%. MS1 spectra were collected using a scan range of 400–1600 *m*/*z*, 120k resolution, AGC target of 300%, and automatic injection times. Data-dependent MS2 spectra were obtained using a monoisotopic peak selection mode: peptide, including charge state 2–7, TopSpeed method (3s cycle time), isolation window 0.4 *m*/*z*, HCD fragmentation using a normalized collision energy of 36%, 45k resolution, AGC target of 200%, automatic maximum injection times, and a dynamic exclusion (20 ppm window) set to 60s.

Peptide Identification and Quantification

Identification and quantification of peptides were performed in Proteome Discoverer 2.4 (Thermo Fisher) using the SwissProt human database (TaxID 9606, released 11/23/2019; 42,252 entries searched) with nsp3.1, nsp4, orf8, CFTR, hERG-HA, and PMP22-Myc sequences (6 entries) manually added (42,258 total entries searched). Searches were conducted with Sequest HT using the following parameters: trypsin cleavage (maximum

two missed cleavages), minimum peptide length 6 AAs, precursor mass tolerance 20 ppm, fragment mass tolerance 0.02 Da, dynamic modifications of Met oxidation (+15.995 Da), protein N-terminal Met loss (−131.040 Da), and protein N-terminal acetylation (+42.011 Da), static modifications of TMTpro (+304.207 Da) at Lys, and N-termini and Cys carbamidomethylation (+57.021 Da). Peptide IDs were filtered using Percolator with an FDR target of 0.01. Proteins were filtered based on a 0.01 FDR, and protein groups were created according to a strict parsimony principle. TMT reporter ions were quantified considering unique and razor peptides, excluding peptides with coisolation interference greater than 25%. Peptide abundances were normalized based on total peptide amounts in each channel, assuming similar levels of background. Protein quantification used all quantified peptides. Postsearch filtering was carried out to include only proteins with two or more identified peptides. Common contaminants (e.g., albumin and keratins) were flagged and not included in downstream analyses.

Data Availability

The mass spectrometry proteomics data have been deposited to the ProteomeXchange Consortium via the PRIDE partner repository with the data set identifier PXD039797. All other necessary data are contained within the manuscript.

RESULTS AND DISCUSSION

SARS-CoV-2 nsp4 Upregulates Expression of UPR Reporter Proteins

Given the role of nsp4 in modulating host ER membranes during infection, we hypothesized that nsp4 may induce ER stress and subsequently activate the UPR pathway. To test this, we exogenously expressed a C-terminally FLAG-tagged SARS-CoV-2 nsp4 construct (nsp4-FT, Figure 1a) in HEK293T cells as previously reported[21] and measured transcript and protein expression of several UPR branch markers. Tdtomato (Tdt) expression was used as a negative control to account for any transfection-induced cell stress and to benchmark the basal state of UPR marker levels. Importantly, previous work has shown transient expression of fluorescent, cytosolic proteins does not induce ER stress and the UPR.[30] Treatment with tunicamycin (Tm, 1 μg/mL, 6 h) was used as a positive control for strong general UPR activation. Samples were harvested 40 h post-transfection, to ensure robust expression of viral proteins. Using RT-qPCR, we found that nsp4-FT expression led to a moderate but signification upregulation of *HSPA5* transcripts and upregulation, though not significantly, of *PDIA4* transcripts, both markers for ATF6 branch-activation[6,11,31] (Figure 1b).

To probe downstream protein expression of ATF6 UPR markers, we measured BiP, GRP94, and PDIA4 levels by western blotting in the presence of nsp4-FT (Figure 1c,d,e,f, Supplemental Figure S1, S2). These proteins have been extensively used in prior studies as western blot markers for ATF6.[32] Quantification of the control and nsp4-FT lanes shows that nsp4 induces a weak upregulation of ATF6 reporter proteins (Figure 1d,f). We also found that nsp4-FT induces upregulation of a PERK pathway marker, CHOP[33] (Figure 1e,f, Supplemental Figure S2), to a greater extent than SARS-CoV-2 FT-nsp2 (a cytosolic viral protein).

To determine whether nsp4-induced CHOP upregulation is mediated through the PERK pathway as opposed to other stress pathways, such as the Integrated Stress Response (ISR) pathway, we utilized the PERK inhibitor GSK2656157 (PERKi).[34,35] In HEK293T cells, GFP transfection with DMSO treatment served as basal control, and Tm (1 μg/mL, 16 h) with PERKi treatment (1 μM, 16 h) was used as positive control for PERK inhibition activity. We found that treating cells expressing nsp4-FT with PERKi reduces induction of an upstream transcriptional regulator of CHOP, ATF4, (Supplemental Figure S3), indicating that nsp4 upregulation of the ATF4/CHOP axis is dependent on PERK.

Together, these results indicate that SARS-CoV-2 nsp4 activates the UPR, albeit at milder levels than the toxic ER stressor tunicamycin but still at biologically relevant levels.

Nsp4 Upregulates the ATF6 and PERK Pathways as Measured by Quantitative Proteomics

While measuring a select few protein markers by western blotting provides some indication of UPR activation, a more precise and pathway-wide approach is required to comprehensively characterize the downstream modulation of the cellular proteome. To this end, we analyzed the global proteome of HEK293T cells transfected with SARS-CoV-2 nsp4-StrepTag (nsp4-ST) using tandem mass spectrometry (LC-MS/MS) with TMTpro isobaric tags to quantify protein abundance (Figure 2a, Supplemental Tables S1–S3). Transfection of GFP was used as a control to indicate the basal state of UPR (-nsp4). Samples were normalized based on global peptide abundance (Supplemental Figure S4). Over 4,200 proteins were identified, with HSPA5 being the most upregulated host protein (Figure 2b). A ranked list enrichment analysis of Gene Ontology (GO) Biological Processes terms identified “Cytoplasmic Translation” (GO:0002181) as the only GO term significantly enriched, with the majority of these categorized proteins positively enriched in the presence of nsp4 (Supplemental Figure S5).

To measure pathway-wide changes of each UPR branch, we used a previously defined set of genes that have been shown to be transcriptionally upregulated upon stress-independent activation by RNA-Seq analysis[6,24,36] (Supplemental Table S1). By quantifying proteome changes in these pathway reporters, we can account for viral protein-mediated alterations in translation or degradation of proteostasis factors that may occur downstream of transcriptional activation.

We compared UPR pathway upregulation in the absence or presence of nsp4 by examining the distribution of target upregulation for each pathway (Figure 2c, Supplemental Figure S6). We found that both the ATF6 and PERK pathways were significantly upregulated.

We also examined the abundances of individual proteins identified within the ATF6 and PERK pathways (Figure 2d). There was a heterogeneous ATF6 response to nsp4 expression, with some proteins (DNAJB11 and MANF) displaying relatively small change, while others (HSPA5, PDIA4, HYOU1, HSP90B1) showed much higher upregulation. Comparing to previously published proteomics data set,[22] we find nsp4-ST induces higher expression of ATF6 markers over basal levels compared to a specific ATF6 pharmacological activator, compound 147, but to a lesser extent than Tm treatment (Supplemental Figure S7). We

found that the upregulation of the PERK pathway by nsp4 was largely dominated by changes in ASNS and WARS abundance (Figure 2d).

To determine whether UPR activation by nsp4 was simply a result of overexpressing a multipass transmembrane protein, we expressed a panel of proteins with similar topology properties in HEK293T cells and measured effects on UPR markers by TMTpro LC/MS-MS compared to nsp4 and a GFP control (Supplemental Figure S8, Supplemental Tables S4 and S5). We chose multipass transmembrane proteins with previously characterized roles in human disease, specifically wild-type Cystic Fibrosis Transmembrane Conductance Regulator (CFTR),[28] HA-tagged human Ether-à-go-go-Related Gene (hERG-HA),[26] and Myc-tagged Peripheral Myelin Protein 22 (PMP22-Myc).[27] None of these transmembrane proteins activated the UPR to an extent similar to that of nsp4, most notably the ATF6 pathway, indicating an nsp4-specific phenotype.

To determine if this phenotype extends to disease-relevant cell models, we expressed SARS-CoV-2 nsp4-FT in A549 lung epithelial cells and measured changes in UPR markers via TMTpro LC/MS-MS (Figure 2e, Supplemental Figure S4, S9, S10, Supplemental Tables S6 and S7). As a positive control for UPR activation, we included samples treated with Tm (1 μg/mL for 16 h). In our proteomics data set, we identified close to 4,000 proteins, with only one host protein surpassing a Log2 fold change > 1 threshold (AHSG) (Supplemental Figure S9). A ranked list enrichment GO term analysis identified several terms significantly enriched, including “Nuclear DNA replication” and “Regulation of chromosome separation” (Supplemental Figure S9).

ATF6 protein markers are moderately but statistically significantly increased in the presence of nsp4, though to a lesser extent than in HEK293T cells, while the PERK pathway was not up-regulated but rather down-regulated, indicative of some cell-type specific effects. Together, these results indicate that SARS-CoV-2 nsp4 activates an ATF6 and PERK response characterized by substantial ER chaperone upregulation, though to a lesser extent compared to the potent ER stressor, tunicamycin.

SARS-CoV-2 nsp3.1 Suppresses nsp4-Induced PERK Activation but Not ATF6 Activation

Nsp4 and nsp3 are key inducers of double-membrane vesicle (DMV) formation during CoV replication,[16,19] which, along with viral protein production, may induce ER stress and the UPR. We previously showed an N-terminal fragment of nsp3 (nsp3.1) suppresses pharmacological ATF6 activation.[22] Therefore, we sought to test whether nsp3.1 might dampen nsp4-induced UPR activation, providing a form of viral tuning of the host UPR. To this end, we cotransfected HEK293T cells with SARS-CoV-2 nsp4-ST and nsp3.1-FT plasmids in equal amounts (0.75 μg) and measured the effect on ATF6 protein reporters by Western blot and UPR markers by mass spectrometry (Figure 3a, Supplemental Tables S2 and S3). In addition, we tested if nsp3.1 could suppress UPR activation induced by SARS-CoV-2 orf8-ST, another viral protein known to activate the UPR[3]. A GFP transfection served as a control for basal UPR state. To ensure that all samples were expressing similar amounts of protein, individual viral protein transfections were supplemented with equal amounts of GFP-expression plasmid (0.75 μg each). All transfections used 1.5 μg DNA plasmid in total.

As expected, we found that transfection with nsp4 and orf8 individually induced increased protein expression of the ATF6 markers BiP and GRP94 (though not PDIA4) compared to basal conditions, as measured by western blotting (Figure 3b,c, Supplemental Figure S11). However, nsp3.1 did not lead to any notable decrease in the expression of ATF6 markers when coexpressed with nsp4 or orf8.

To more comprehensively quantify UPR protein markers, we analyzed these same lysates by TMTpro-quantitative LC-MS/MS. We found that nsp3.1 does not suppress nsp4-or orf8-induced ATF6 activation (Figure 3d). Interestingly, we found that coexpression of nsp3.1 with nsp4 significantly lowers PERK marker levels compared to nsp4 alone (Figure 3e), while IRE1/XBP1s activation was not significantly decreased with coexpression (Supplemental Figure S12). These results demonstrate that nsp3.1 is not capable of suppressing ATF6 activation induced by other viral proteins, such as nsp4 and orf8, but can suppress PERK activation.

Curiously, we also noted nsp3.1 protein levels are lower in cotransfections with nsp4 versus GFP, as seen by both western blotting (Figure 3b, quantified in Supplemental Figure S13) and proteomics (Supplemental Figure S13). Examining global changes in the proteome with nsp4 expression showed few proteins are substantially down-or up-regulated (Supplemental Figure S5). Therefore, it is likely that this is a specific effect on nsp3.1 protein levels.

Reanalysis Shows Time-Dependent PERK Activation during SARS-CoV-2 Infection

Previous work has shown that the UPR is activated during SARS-CoV-2 infection.[3] A reanalysis of global proteomics during a SARS-CoV-2 infection time-course in Caco-2 cells[37] shows a modest upregulation of ATF6 and IRE1/XBP1s pathways by 10 hpi (Figure 4a–d). Additionally, a moderate upregulation of PERK-induced protein markers at 6 hpi is downregulated by 24 hpi (Figure 4e,f), particularly for ABCF2, ASNS, CEBPB, and SLC1A4. This time-dependent regulation of the PERK UPR pathway induction and subsequent suppression may be explained by nsps, such as nsp3.1 and nsp4. Early activation of the PERK pathway may be important to interfere with host translation through eIF2α phosphorylation, while the later deactivation would avoid ATF4/CHOP-mediated cell death typically associated with prolonged PERK activation.

CONCLUSIONS

Previous studies show that SARS-CoV-2, SARS-CoV, and MHV activate branches of the UPR to varying degrees[2–4,14,15]; however, the role of nsps in this process has remained largely unexplored. Of particular interest are the nsps involved in host membrane alteration to promote infection by DMV formation such as nsp3 and nsp4. In this work, we find that overexpression of SARS-CoV-2 nsp4 activates the ATF6 and PERK branches of the UPR in HEK293T cells (Figures 1 and 2). This is evident by western blotting for both ATF6 markers such as BiP and GRP94 and PERK marker CHOP (Figure 1).

We further harnessed the capabilities of TMTpro-based quantitative proteomics to measure the pathway changes in these UPR branches. The grouped analysis of coregulated protein sets for the individual UPR pathways enables a comparative assessment of the degree of

UPR branch activation and can even detect very small levels of induction (Figure 2). We also find that nsp4 activates the ATF6 pathway in A549 cells, though more moderately compared to HEK293T cells (Figure 2e), indicating cell-specific effects that may be tied to variable nsp4 protein expression in different cells, or divergent regulation mechanism of the UPR. We also acknowledge that transient transfection of individual or pairs of viral proteins cannot completely reflect the complete infection milieu; however, this reductionist approach allows for characterization of specific viral protein contributions to UPR modulation, as has been conducted in prior studies.[3,14,15]

In both HEK293T and A549 cells, the overall degree of UPR activation by nsp4 is lower than with the highly toxic, global ER stressor tunicamycin, but higher than treatment with branch specific pharmacologic activators (Figure 2, Supplemental Figure S7). This is in line with the moderate UPR activation observed in viral infection, where strong, chronic UPR activation may trigger apoptosis and would likely be counterproductive for replication. Additionally, prior work has found that modest upregulation of individual UPR branches can substantially improve quality control and secretion of disease-relevant proteins, such as in light-chain amyloido-sis.[23,24] Furthermore, our use of TMTpro-based quantitative proteomics using reporter ion intensity from MS2 spectra is subject to ratio compression, which may reduce the magnitude of observed fold changes.[38] Thus, the moderate UPR activation measured here may be biologically relevant to the CoV-reprogramming of host cells during infection.

It is pertinent to further study the molecular mechanisms by which nsp4 triggers UPR activation. We have previously profiled a comparative interactome of nsp4 homologues[21] and did not identify protein interactions with the ATF6 sensor protein as seen with nsp3,[22] making it unlikely that signaling occurs through a direct interaction. As a multipass transmembrane protein, nsp4 may be prone to misfolding or may modulate host ER membranes, which can trigger ATF6 activation in some cases.[39] Further work is needed to define the precise molecular mechanisms by which nsp4 activates the ATF6 and PERK branches.

We previously showed that an N-terminal fragment of SARS-CoV-2 nsp3, nsp3.1, interacts with ATF6 and can suppress pharmacological activation of the ATF6 pathway.[22] We hypothesized that nsp3 and nsp4 may act in concert to tune the UPR to increase the protein folding capacity while minimizing the apoptotic effects of chronic activation. We found that coexpression of nsp3.1 with nsp4 or orf8 does not repress ATF6 activation but does suppress nsp4-induced PERK activation (Figure 3). Time-dependent PERK activation was evident from global proteomics data during SARS-CoV-2 infection[37] showing an increase in target protein levels during the first 6 hpi, followed by a later decline (Figure 4). Though the magnitude of pathway change was more subdued than our data set, partially due to noisier data, there is still a trend of tight temporal regulation. This suggests a role for nsp3 and nsp4 in moderating PERK signaling to permit early signaling events (eIF2α-mediated host translational attenuation) that are beneficial for viral propagation while preventing ATF4/CHOP-mediated induction of apoptosis.

The precise mechanism by which nsp3.1 suppresses nsp4-induced PERK activation will require further investigation. SARS-CoV-2 nsp3.1 directly interacts with ATF3,[22] a PERK protein marker which is upregulated by ATF4 and promotes pro-apoptotic signaling.[40] This protein interaction may represent one avenue by which the PERK pathway is tuned by nsp3.1 to limit apoptosis in infected cells. We also acknowledge that other kinases, such as those involved in the Integrated Stress Response (ISR), may be activated, contributing to the upregulation of protein markers categorized under the PERK pathway. We do find that nsp4-mediated upregulation of these proteins is dependent on PERK, using a small molecule PERK inhibitor (GSK2656157) (Supplemental Figure S3). However, the contributions of other kinases, particularly in the context of our reanalysis of infection-based proteomics, cannot be ruled out.

The absence of ATF6 suppression in coexpression is surprising, given that we previously showed nsp3.1 could suppress ATF6 activation by tunicamycin treatment, which potently activates the global UPR through inhibition of protein glycosylation. This may suggest that the mechanisms by which nsp4 activates the ATF6 pathway are distinct from those of a general tunicamycin stressor and can overcome the opposing effects of nsp3.1. Alternatively, nsp4-induced ATF6 activation may be too moderate for nsp3.1 to have any measurable effect (Supplemental Figure S7). In the context of viral infection, there are multiple points of UPR induction via nsp4, orf8, Spike, ER membrane perturbation, etc., which in combination may require partial suppression by nsp3.1 to tune the host UPR and prevent host cell apoptosis.

Relatedly, coexpression of nsp4 with nsp3.1 leads to a noticeable decrease of nsp3.1 levels compared to control coexpression of GFP with nsp3.1 (Figure 3b, Supplemental Figure S13). This drop in protein levels may in part explain the lack of suppression of ATF6 by nsp3.1. It is unclear how nsp4 affects the nsp3.1 levels. While ATF6 activation increases the production of ERAD factors to clear misfolded proteins, nsp3.1 is a cytosolic fragment of nsp3 and should not be subject to increased ERAD.

Additional questions remain regarding nsps and the UPR, such as how conserved is UPR activation across nsp4 homologues? Does nsp6, another key protein in DMV formation,[16] have a similar effect on the UPR? And how might nsp3, nsp4, and nsp6 affect the UPR in concert? Using quantitative proteomics to measure changes in UPR-induced protein expression, as we have done here, should prove to be a powerful and comprehensive tool in answering these questions.

Lastly, previous work has shown that UPR inhibition can attenuate SARS-CoV-2[3] and MERS-CoV[41] infection. Viral families beyond coronaviruses, such as flaviviruses, have been shown to rely on the UPR and can be inhibited using UPR modulators.[42–44] These opposing phenotypes, in which either UPR activation or inhibition can disrupt infection, highlight the important and diverse roles that the UPR plays in viral replication. Continued efforts to delineate the roles of individual viral proteins in modifying the UPR will be critical to the further development of UPR-targeting antivirals. Our work contributes to this goal by identifying a new role for SARS-CoV-2 nsp4 as a potent UPR activator and the coordination of nsp3.1 with nsp4 to tune the PERK pathway.

Supplementary Material

Refer to Web version on PubMed Central for supplementary material.

ACKNOWLEDGMENTS

We thank Dr. Nevan Krogan (University of California, San Francisco) for the pLVX-EF1alpha-SARS-CoV-2-nsp2-2xStrepTag plasmid and Dr. Joseph Genereux (University of California, Riverside) for cell stocks. We thank Drs. Eric Sorcher and Jeong Hong (Emory University) for the WT-CFTR plasmid, Dr. Brett Kronke (Vanderbilt University Medical Center) for the hERG-HA plasmid, and Dr. Charles Sanders (Vanderbilt University) for the PMP22-Myc plasmid. We thank members of the Plate lab for their critical reading and feedback on this manuscript. Work was funded by R35GM133552 (National Institute of General Medical Sciences) and Vanderbilt University start-up funds. J.P.D. was supported by T32GM008554 (National Institute of General Medical Sciences). B.K.R. was supported by T32GM137793 and T32GM139800 (National Institute of General Medical Sciences). R.J.H.W. was supported by R01DK107944 (National Institute of Diabetes and Digestive and Kidney Diseases) and R01GM121621 (National Institute of General Medical Sciences).

REFERENCES

(1). WHO. Weekly Epidemiological Update on COVID-19. W. H. O 2020, 1, 4.

(2). Xue M; Feng L The Role of Unfolded Protein Response in Coronavirus Infection and Its Implications for Drug Design. Front. Microbiol 2021, 12, No. 808593, DOI: 10.3389/fmicb.2021.808593.

(3). Echavarría-Consuegra L; Cook GM; Busnadiego I; Lefèvre C; Keep S; Brown K; Doyle N; Dowgier G; Franaszek K; Moore NA; Siddell SG; Bickerton E; Hale BG; Firth AE; Brierley I; Irigoyen N Manipulation of the Unfolded Protein Response: A Pharmacological Strategy against Coronavirus Infection. PLOS Pathog. 2021, 17 (6), No. e1009644.

(4). Bechill J; Chen Z; Brewer JW; Baker SC Coronavirus Infection Modulates the Unfolded Protein Response and Mediates Sustained Translational Repression. J. Virol 2008, 82 (9), 4492–4501. [PubMed: 18305036]

(5). Walter P; Ron D The Unfolded Protein Response: From Stress Pathway to Homeostatic Regulation. Science (80-.) 2011, 334 (6059), 1081–1086.

(6). Shoulders MD; Ryno LM; Genereux JC; Moresco JJ; Tu PG; Wu C; Yates JR; Su AI; Kelly JW; Wiseman RL Stress-Independent Activation of XBP1s and/or ATF6 Reveals Three Functionally Diverse ER Proteostasis Environments. Cell Rep. 2013, 3 (4), 1279–1292. [PubMed: 23583182]

(7). Szegezdi E; Logue SE; Gorman AM; Samali A Mediators of Endoplasmic Reticulum Stress-induced Apoptosis. EMBO Rep. 2006, 7 (9), 880–885. [PubMed: 16953201]

(8). Harding HP; Zhang Y; Bertolotti A; Zeng H; Ron D Perk Is Essential for Translational Regulation and Cell Survival during the Unfolded Protein Response. Mol. Cell 2000, 5 (5), 897–904. [PubMed: 10882126]

(9). Lee A-H; Iwakoshi NN; Glimcher LH XBP-1 Regulates a Subset of Endoplasmic Reticulum Resident Chaperone Genes in the Unfolded Protein Response. Mol. Cell. Biol 2003, 23 (21), 7448–7459. [PubMed: 14559994]

(10). Haze K; Yoshida H; Yanagi H; Yura T; Mori K Mammalian Transcription Factor ATF6 Is Synthesized as a Transmembrane Protein and Activated by Proteolysis in Response to Endoplasmic Reticulum Stress. Mol. Biol. Cell 1999, 10 (11), 3787–3799. [PubMed: 10564271]

(11). Adachi Y; Yamamoto K; Okada T; Yoshida H; Harada A; Mori K ATF6 Is a Transcription Factor Specializing in the Regulation of Quality Control Proteins in the Endoplasmic Reticulum. Cell Struct. Funct 2008, 33 (1), 75–89. [PubMed: 18360008]

(12). Aviner R; Frydman J Proteostasis in Viral Infection: Unfolding the Complex Virus–Chaperone Interplay. Cold Spring Harb. Perspect. Biol 2020, 12 (3), a034090. [PubMed: 30858229]

(13). Fung TS; Liu DX Coronavirus Infection, ER Stress, Apoptosis and Innate Immunity. Front. Microbiol 2014, 5, 296 DOI: 10.3389/fmicb.2014.00296. [PubMed: 24987391]

(14). Minakshi R; Padhan K; Rani M; Khan N; Ahmad F; Jameel S The SARS Coronavirus 3a Protein Causes Endoplasmic Reticulum Stress and Induces Ligand-Independent Downregulation of the Type 1 Interferon Receptor. PLoS One 2009, 4 (12), No. e8342.

(15). Sung S-C; Chao C-Y; Jeng K-S; Yang J-Y; Lai MMC The 8ab Protein of SARS-CoV Is a Luminal ER Membrane-Associated Protein and Induces the Activation of ATF6. Virology 2009, 387 (2), 402–413. [PubMed: 19304306]

(16). Angelini MM; Akhlaghpour M; Neuman BW; Buchmeier MJ Severe Acute Respiratory Syndrome Coronavirus Nonstructural Proteins 3, 4, and 6 Induce Double-Membrane Vesicles. MBio 2013, 4 (4), 1–10.

(17). Lei J; Kusov Y; Hilgenfeld R Nsp3 of Coronaviruses: Structures and Functions of a Large Multi-Domain Protein. Antiviral Res. 2018, 149, 58–74. [PubMed: 29128390]

(18). Shin D; Mukherjee R; Grewe D; Bojkova D; Baek K; Bhattacharya A; Schulz L; Widera M; Mehdipour AR; Tascher G; Geurink PP; Wilhelm A; van der Heden van Noort GJ; Ovaa H; Müller S; Knobeloch K-P; Rajalingam K; Schulman BA; Cinatl J; Hummer G; Ciesek S; Dikic I Papain-like Protease Regulates SARS-CoV-2 Viral Spread and Innate Immunity. Nature 2020, 587 (7835), 657–662. [PubMed: 32726803]

(19). Oostra M; te Lintelo EG; Deijs M; Verheije MH; Rottier PJM; de Haan CAM Localization and Membrane Topology of Coronavirus Nonstructural Protein 4: Involvement of the Early Secretory Pathway in Replication. J. Virol 2007, 81 (22), 12323–12336. [PubMed: 17855519]

(20). Beachboard DC; Anderson-Daniels JM; Denison MR Mutations across Murine Hepatitis Virus Nsp4 Alter Virus Fitness and Membrane Modifications. J. Virol 2015, 89 (4), 2080–2089. [PubMed: 25473044]

(21). Davies JP; Almasy KM; McDonald EF; Plate L Comparative Multiplexed Interactomics of SARS-CoV-2 and Homologous Coronavirus Nonstructural Proteins Identifies Unique and Shared Host-Cell Dependencies. ACS Infect. Dis 2020, 6, 3174–3189. [PubMed: 33263384]

(22). Almasy KM; Davies JP; Plate L Comparative Host Interactomes of the SARS-CoV-2 Nonstructural Protein 3 and Human Coronavirus Homologs. Mol. Cell. Proteomics 2021, 20, No. 100120.

(23). Plate L; Rius B; Nguyen B; Genereux JC; Kelly JW; Wiseman RL Quantitative Interactome Proteomics Reveals a Molecular Basis for ATF6-Dependent Regulation of a Destabilized Amyloidogenic Protein. Cell Chem. Biol 2019, 26, 913–925.e4. [PubMed: 31105062]

(24). Plate L; Cooley CB; Chen JJ; Paxman RJ; Gallagher CM; Madoux F; Genereux JC; Dobbs W; Garza D; Spicer TP; Scampavia L; Brown SJ; Rosen H; Powers ET; Walter P; Hodder P; Wiseman RL; Kelly JW Small Molecule Proteostasis Regulators That Reprogram the ER to Reduce Extracellular Protein Aggregation. eLife 2016, 5, No. e15550.

(25). Sabusap CM; Wang W; McNicholas CM; Chung WJ; Fu L; Wen H; Mazur M; Kirk KL; Collawn JF; Hong JS; Sorscher EJ Analysis of Cystic Fibrosis–Associated P67L CFTR Illustrates Barriers to Personalized Therapeutics for Orphan Diseases. JCI Insight 2016, 1 (14), 1–10.

(26). Kozek KA; Glazer AM; Ng C-A; Blackwell D; Egly CL; Vanags LR; Blair M; Mitchell D; Matreyek KA; Fowler DM; Knollmann BC; Vandenberg JI; Roden DM; Kroncke BM High-Throughput Discovery of Trafficking-Deficient Variants in the Cardiac Potassium Channel KV11.1. Hear. Rhythm 2020, 17 (12), 2180–2189.

(27). Marinko JT; Carter BD; Sanders CR Direct Relationship between Increased Expression and Mistrafficking of the Charcot–Marie–Tooth–Associated Protein PMP22. J. Biol. Chem 2020, 295 (34), 11963–11970. [PubMed: 32647009]

(28). McDonald EF; Sabusap CMP; Kim M; Plate L Distinct Proteostasis States Drive Pharmacologic Chaperone Susceptibility for Cystic Fibrosis Transmembrane Conductance Regulator Misfolding Mutants. Mol. Biol. Cell 2022, 33 (7), 1–17.

(29). Fonslow BR; Niessen SM; Singh M; Wong CCL; Xu T; Carvalho PC; Choi J; Park SK; Yates JR Single-Step Inline Hydroxyapatite Enrichment Facilitates Identification and Quantitation of Phosphopeptides from Mass-Limited Proteomes with MudPIT. J. Proteome Res 2012, 11 (5), 2697–2709. [PubMed: 22509746]

(30). Simic MS; Moehle EA; Schinzel RT; Lorbeer FK; Halloran JJ; Heydari K; Sanchez M; Jullié D; Hockemeyer D; Dillin A Transient Activation of the UPR ER Is an Essential Step in the Acquisition of Pluripotency during Reprogramming. Sci. Adv 2019, 5 (4), 1–13.

(31). Ye J; Rawson RB; Komuro R; Chen X; Davé UP; Prywes R; Brown MS; Goldstein JL ER Stress Induces Cleavage of Membrane-Bound ATF6 by the Same Proteases That Process SREBPs. Mol. Cell 2000, 6 (6), 1355–1364. [PubMed: 11163209]

(32). Schröder M; Kaufman RJ THE MAMMALIAN UNFOLDED PROTEIN RESPONSE. Annu. Rev. Biochem 2005, 74 (1), 739–789. [PubMed: 15952902]

(33). Marciniak SJ; Yun CY; Oyadomari S; Novoa I; Zhang Y; Jungreis R; Nagata K; Harding HP; Ron D CHOP Induces Death by Promoting Protein Synthesis and Oxidation in the Stressed Endoplasmic Reticulum. Genes Dev. 2004, 18 (24), 3066–3077. [PubMed: 15601821]

(34). Axten JM; Romeril SP; Shu A; Ralph J; Medina JR; Feng Y; Li WHH; Grant SW; Heerding DA; Minthorn E; Mencken T; Gaul N; Goetz A; Stanley T; Hassell AM; Gampe RT; Atkins C; Kumar R Discovery of GSK2656157: An Optimized PERK Inhibitor Selected for Preclinical Development. ACS Med. Chem. Lett 2013, 4 (10), 964–968. [PubMed: 24900593]

(35). Atkins C; Liu Q; Minthorn E; Zhang S-Y; Figueroa DJ; Moss K; Stanley TB; Sanders B; Goetz A; Gaul N; Choudhry AE; Alsaid H; Jucker BM; Axten JM; Kumar R Characterization of a Novel PERK Kinase Inhibitor with Antitumor and Antiangiogenic Activity. Cancer Res. 2013, 73 (6), 1993–2002. [PubMed: 23333938]

(36). Grandjean JMD; Plate L; Morimoto RI; Bollong MJ; Powers ET; Wiseman RL Deconvoluting Stress-Responsive Proteostasis Signaling Pathways for Pharmacologic Activation Using Targeted RNA Sequencing. ACS Chem. Biol 2019, 14 (4), 784–795. [PubMed: 30821953]

(37). Bojkova D; Klann K; Koch B; Widera M; Krause D; Ciesek S; Cinatl J; Münch C Proteomics of SARS-CoV-2-Infected Host Cells Reveals Therapy Targets. Nature 2020, 583, 469–472. [PubMed: 32408336]

(38). Ting L; Rad R; Gygi SP; Haas W MS3 Eliminates Ratio Distortion in Isobaric Multiplexed Quantitative Proteomics. Nat. Methods 2011, 8 (11), 937–940. [PubMed: 21963607]

(39). Volmer R; van der Ploeg K; Ron D Membrane Lipid Saturation Activates Endoplasmic Reticulum Unfolded Protein Response Transducers through Their Transmembrane Domains. Proc. Natl. Acad. Sci 2013, 110 (12), 4628–4633. [PubMed: 23487760]

(40). Edagawa M; Kawauchi J; Hirata M; Goshima H; Inoue M; Okamoto T; Murakami A; Maehara Y; Kitajima S Role of Activating Transcription Factor 3 (ATF3) in Endoplasmic Reticulum (ER) Stress-Induced Sensitization of P53-Deficient Human Colon Cancer Cells to Tumor Necrosis Factor (TNF)-Related Apoptosis-Inducing Ligand (TRAIL)-Mediated Apoptosis through Up-Regulation of Death Receptor 5 (DR5) by Zerumbone and Celecoxib. J. Biol. Chem 2014, 289 (31), 21544–21561. [PubMed: 24939851]

(41). Sims AC; Mitchell HD; Gralinski LE; Kyle JE; Burnum-Johnson KE; Lam M; Fulcher ML; West A; Smith RD; Randell SH; Metz TO; Sheahan TP; Waters KM; Baric RS Unfolded Protein Response Inhibition Reduces Middle East Respiratory Syndrome Coronavirus-Induced Acute Lung Injury. MBio 2021, 12 (4), 1–22.

(42). Peña J; Harris E Dengue Virus Modulates the Unfolded Protein Response in a Time-Dependent Manner. J. Biol. Chem 2011, 286 (16), 14226–14236. [PubMed: 21385877]

(43). Almasy KM; Davies JP; Lisy SM; Tirgar R; Tran SC; Plate L Small-Molecule Endoplasmic Reticulum Proteostasis Regulator Acts as a Broad-Spectrum Inhibitor of Dengue and Zika Virus Infections. Proc. Natl. Acad. Sci. U. S. A 2021, 118 (3), 1–12.

(44). Kolpikova EP; Tronco AR; Den Hartigh AB; Jackson KJ; Iwawaki T; Fink SL IRE1α Promotes Zika Virus Infection via XBP1. Viruses 2020, 12 (3), 278. [PubMed: 32138181]

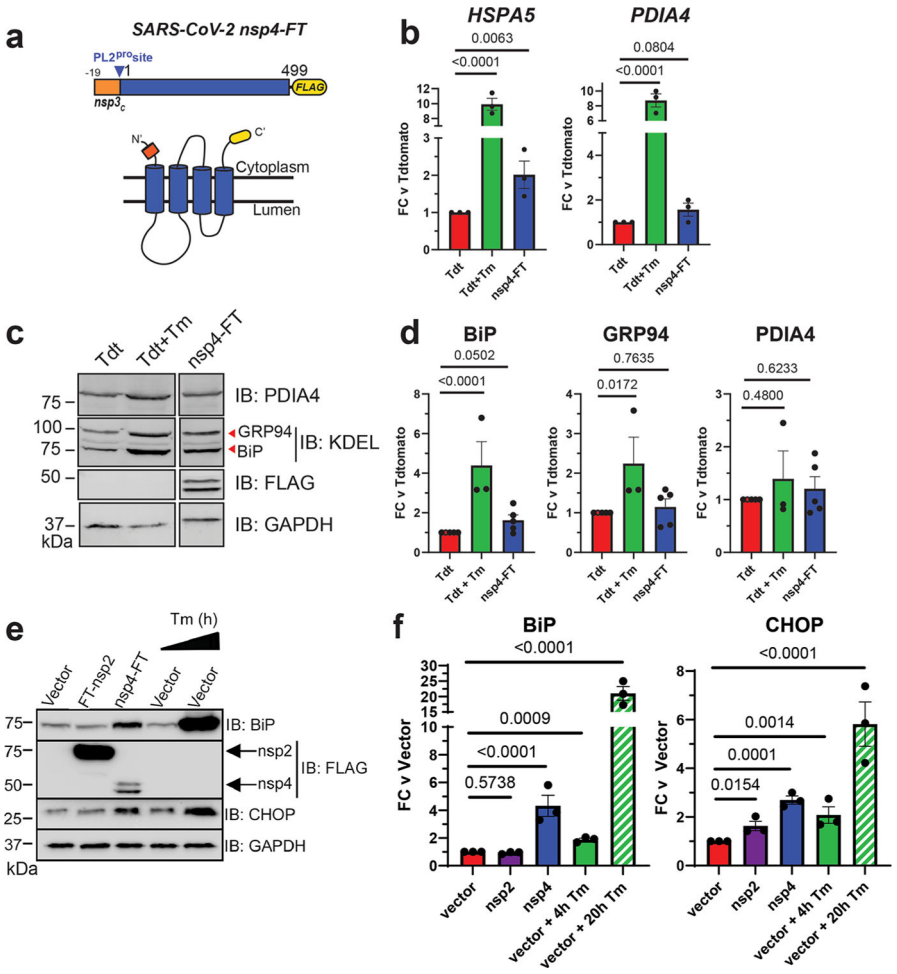

Figure 1.

SARS-CoV-2 nsp4 upregulates the expression of UPR reporter proteins. (a) SARS-CoV-2 nsp4 expression construct and membrane topology, containing a C-terminal FLAG-tag (nsp4-FT) and an N-terminal segment of the last 19 C-terminal amino acids in nsp3 for optimal membrane insertion.[21] Construct contains the native $PL2^{pro}$ protease cleavage site. (b) RT-qPCR of ATF6 pathway activation reporters *HSPA5* and *PDIA4* in the presence of SARS-CoV-2 nsp4-FT, normalized to *GAPDH* transcripts and compared to basal levels (GFP). Treatment with 1 μg/mL Tunacimycin (Tm) for 6 h was used as a positive control. n = 3, mean ± SEM, one-way ANOVA with Benjamini, Krieger, and Yekutieli multiple testing correction, $p < 0.05$ considered statistically significant. (c) Representative western blot of ATF6 protein markers (PDIA4, GRP94, BiP) in the presence of Tdtomato (Tdt), SARS-CoV-2 nsp4-FT, or treatment with 1 μg/mL Tm (16 h), with GAPDH as a housekeeping gene for loading control. Displayed blot sections are from the same blot image and exposure settings (see Supplemental Figure S1 for all quantified, original blots). (d) Quantification of Tdtomato (Tdt), and nsp4-FT in western blots in panel (c), normalized to GAPDH band intensities, and compared to basal levels (Tdt). n = 3–5, mean ± SEM, one-way ANOVA with Benjamini, Krieger, and Yekutieli multiple testing correction, $p < 0.05$ considered statistically significant. (e) Representative western blot of CHOP and BiP in the presence of SARS-CoV-2 FT-nsp2, nsp4-FT, or treatment with 5 μg/mL Tm for short (4h) or long (20h)

time points. See Supplemental Figure S2 for all quantified, original blots. (f) Quantification of western blots in panel (e), normalized to GAPDH band intensities and compared to basal control (vector). $n = 3$, mean ± SEM. One-way ANOVA with Benjamini, Krieger, and Yekutieli multiple testing correction, $p < 0.05$ considered statistically significant.

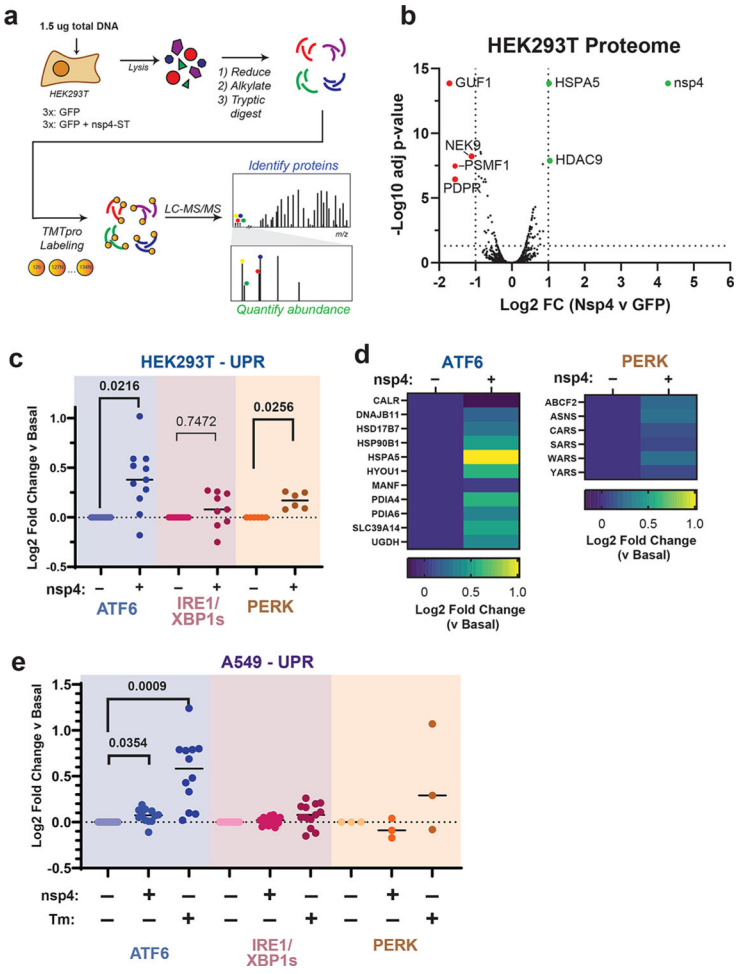

Figure 2.

SARS-CoV-2 nsp4 upregulates the ATF6 and PERK pathways, as measured by quantitative proteomics. (a) Experimental schematic to measure UPR induction by SARS-CoV-2 nsp4-ST expression in HEK293T cells using tandem mass spectrometry (LC/MS-MS) and TMTpro-based quantification. (b) Volcano plot of global proteome changes, with cut-offs indicating Log2 FC (vs GFP) < −1 or > 1, adjusted *p* value < 0.05. Proteins passing cut-offs are annotated. Adjusted *p* value calculated using a *t* test, controlling for FDR by the Benjamini-Hochberg method. $N = 3$, 1 MS run. c) Log2 fold change of UPR branch protein markers in the absence (GFP) or presence of SARS-CoV-2 nsp4-ST, as outlined in panel (a) assessed by TMT reporter ion intensities. Dots represent individual protein markers previously defined by RNA-seq analysis to be transcriptionally upregulated upon stress-independent activation of respective UPR branches.[6,24,36] Swarm plot shows median, $n = 3$ biological replicates, 1 MS run, one-way ANOVA with Geisser–Greenhouse correction and post hoc Tukey's multiple comparison test was used to test significance, $p < 0.05$ considered significant. See Supplemental Tables S2 and S3 for the mass spectrometry data set. (d) Heatmap of individual log2 fold change for ATF6 and PERK protein markers in the absence or presence of SARS-CoV-2 nsp4-ST. (e) Log2 fold change of UPR branch protein markers in A549 lung epithelial cells the presence of SARS-CoV-2 nsp4-FT or tunicamycin (1 μg/mL, 16 h) compared to basal control (GFP). UPR branch protein markers were defined

as in panel (b). Swarm plot shows median, $n = 4$ biological replicates, 1 MS run, one-way ANOVA with Geisser–Greenhouse correction and post hoc Tukey's multiple comparison test was used to test significance, $p < 0.05$ considered significant. See Supplemental Tables S6 and S7 for the mass spectrometry data set.

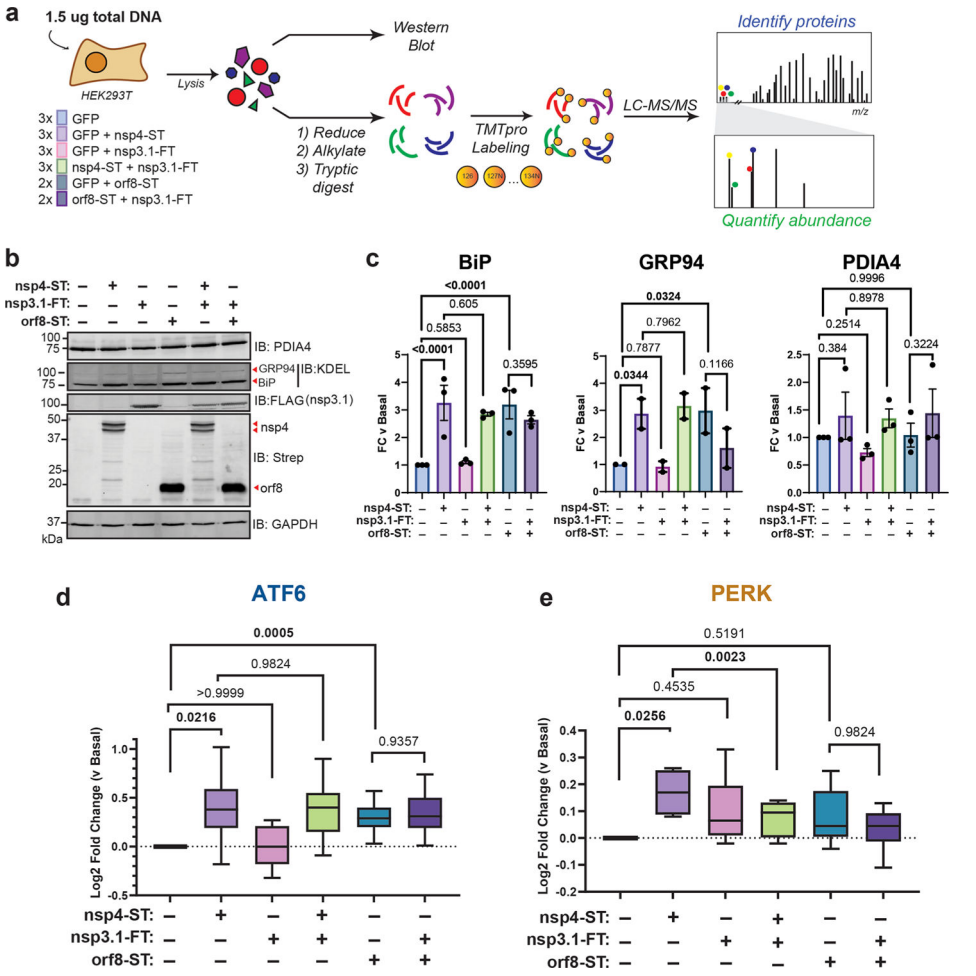

Figure 3.

SARS-CoV-2 nsp3.1 suppresses nsp4-induced PERK, but not ATF6 activation. (a) Experimental schematic to test the effect of SARS-CoV-2 nsp3.1 on nsp4-or orf8-induced activation of the UPR in HEK293T cells by western blotting and tandem mass spectrometry (LC-MS/MS). (b) Representative western blot of ATF6 protein markers (PDIA4, BiP, GRP94) and viral proteins (SARS-CoV-2 nsp4-ST, nsp3.1-FT, and orf8-ST), with GAPDH as a housekeeping gene for a loading control. See Supplemental Figure S11 for all quantified, original blots. (c) Quantification of western blots in panel (b), normalized to GAPDH band intensities. $n = 2–3$, mean ± SEM, One-way ANOVA with Benjamini, Krieger, and Yekutieli multiple testing correction, $p < 0.05$ considered statistically significant. (d) Global proteomics analysis of ATF6 protein marker levels in the presence of SARS-CoV-2 nsp4-ST, nsp3.1-FT, orf8-ST, or specified combinations. Box-and-whisker plot shows median, 25th and 75th quartiles, and minimum and maximum values. One-way ANOVA with Geisser–Greenhouse correction and post hoc Tukey's multiple comparison test was used to test significance; 1 MS run, $n = 2–3$ biological replicates. See Supplemental Tables S2 and S3 for mass spectrometry data set. (e) Global proteomics analysis of PERK protein marker levels, as in panel (d).

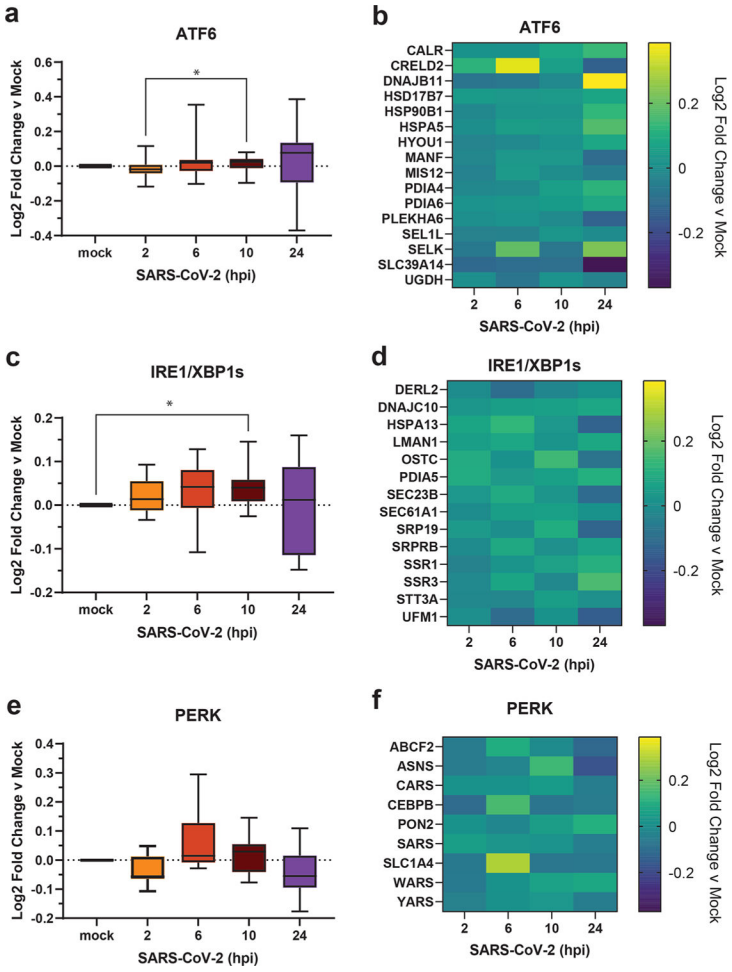

Figure 4.

Reanalysis of UPR activation in global proteomics data of Caco-2 cells infected with SARS-CoV-2. (a, c, e) Box-and-whisker plots of ATF6 (a), IRE1/XBP1s (c), and PERK (e) protein markers during SARS-CoV-2 infection (2–24 h post infection (hpi)) compared to mock infected samples. Box-and-whisker plot shows median, 25th and 75th quartiles, and minimum and maximum values. One-way ANOVA with Geisser–Greenhouse correction and posthoc Tukey's multiple comparison test was used to test significance. **p* value < 0.05 annotated. (b, d, f) Heatmaps of individual ATF6 (b), IRE1/XBP1s (d), and PERK (f) protein markers as in panels (a), (c), and (e), respectively. Data set published by Bojkova et al. 2020.[37]

Table 1.

Description of the Primers Used in This Study[a]

ID	primer	sequence	notes
1	2xStrepTag_rem_F	CTCGAAGGCGGCGGGGGA	amplification of 2xStrepTag from pLVX vector
2	2xStrepTag_rem_R	TTACTTTTCAAACTGCGGATGTGACCATGATCCAC	amplification of 2xStrepTag from pLVX vector
3	nsp4_Wuhan_xFT_F	ATCCGCAGTTTGAAAAGTAATAAACCCGCTGATCAGCC	removal of FLAG tag from nsp4
4	nsp4_Wuhan_xFT_R	CATCCCCCGCCGCCTTCGAGCAGGACTGCGGAAGTAATG	removal of FLAG tag from nsp4
5	Wuhan-orf8_F	CCGGTGAATTCGCCGCCACCATGAAGTTCCTGGTATTTC	amplification of orf8 gene from pcDNA vector
6	Wuhan-orf8_R	CATCCCCCGCCGCCTTCGAGAATAAAGTCCAAGACCAC	amplification of orf8 gene from pcDNA vector
7	pLVX_F	CTCGAAGGCGGCGGGGGA	amplication of pLVX vector with 2xStrepTag
8	pLVX_R	GGTGGCGGCGAATTCACCG	amplication of pLVX vector with 2xStrepTag
9	GAPDH-qPCR_F	GTCGGAGTCAACGGATT	
10	GAPDH-qPCR_R	AAGCTTCCCGTTCTCAG	
11	HSPA5-qPCR_F	GCCTGTATTTCTAGACCTGCC	
12	HSPA5-qPCR_R	TTCATCTTGCCAGCCAGTTG	
13	PDIA4-qPCR_F	AGTGGGGAGGATGTCAATGC	
14	PDIA4-qPCR_R	TGGCTGGGATTTGATGACTG	

[a]Primers are referenced by ID number in the text.